

We are IntechOpen, the world's leading publisher of Open Access books Built by scientists, for scientists

6,900

Open access books available

185,000

International authors and editors

200M

Downloads

Our authors are among the

154

Countries delivered to

TOP 1%

most cited scientists

12.2%

Contributors from top 500 universities



WEB OF SCIENCE™

Selection of our books indexed in the Book Citation Index
in Web of Science™ Core Collection (BKCI)

Interested in publishing with us?
Contact book.department@intechopen.com

Numbers displayed above are based on latest data collected.
For more information visit www.intechopen.com



Thermal Analysis of Phase Transitions and Crystallization in Polymeric Fibers

W. Steinmann, S. Walter, M. Beckers, G. Seide and T. Gries

Additional information is available at the end of the chapter

<http://dx.doi.org/10.5772/54063>

1. Introduction

Each year about 50 Million tons polymer is processed to fibers worldwide [1]. Polymeric fibers are manufactured into all sorts of daily as well as industrial goods [2, 3]. The most prominent materials are thermoplastic among which poly(ethylene terephthalat) (PET), polyamides (PA) and polypropylene (PP) make up the largest fraction [4]. Other thermoplastic polymers such as poly(vinylidene fluoride) (PVDF) belong to niche markets with highly specialized applications [5-7].

The most distinctive property of synthetic fiber materials which separates them from other polymeric products is the strong anisotropic material structure. Geometrically this is characterized by a rather high aspect ratio of diameter to length which can reach several magnitudes of order in filament fibers. An exemplary PET textile multi-filament bundle of 300 single filaments in one flat yarn weighs around 100 g per 10.000 meters length (100 dtex). This yields in a single filament diameter of roughly 3 μm . A common industrial bobbin holds up to 25 kg of a virtually endless length of yarn, which in this case would be 2.5 million meters. The predominant cross section is circular in shape. Nonetheless, depending on the fiber application other cross-sections are possible and also common [3,4].

On a structural level the strong anisotropic character of a thermoplastic fiber is mainly caused and influenced by the production process. Hence, the spinning process of thermoplastic fibers shall be explained briefly. Next to the direct spinning process in which the polymer is directly processed to fibers right after the polymerization process, the most common process is the extruder based fiber production. The polymer granules are heated and transferred into a molten state inside the extruder [8]. The melt is then conveyed into a gear pump which ensures a constant flow of mass. This constant polymer flow then is being pressed through filtration layers and finally extruded through capillaries. Following the extrusion the polymer is drawn down vertically and solidifies while cooling from extrusion

temperature down to the ambient air temperature. Usually the fibers are drawn down mechanically by rollers [4,8]. Figure 1 illustrates a classical melt spinning line. The polymer granules are feed through a hopper (A) into an extruder (B). The molten polymer is transported through heated pipes (C) to a gear pump (D). The gear pump feeds the spin pack (E) in which several layers of filtration are placed. The polymer is then extruded through capillaries and exits the spinpack into the quenching zone (F) where a laminar air flow ensures constant cooling conditions. After solidification and before touching the first roller or godet (H) the filaments are usually coated with a spin finish (G).

The most important process parameters of the melt spinning process are: the extrusion temperature $T_{\text{Extrusion}}$; the mass flow through each single capillary $m_{\text{Throughput}}$; the density of the melt ρ_{Melt} ; the cross-sectional area of the capillary $A_{\text{Capillary}}$; the viscosity η of the melt at the local temperature and the draw down speed v . Of course, there are numerous other parameters that affect the process such as the surface quality of the capillary walls, the form of the capillary rim, the ambient air profile consisting of flow direction, speed and temperature and others. For a basic comprehension these are neglected at this point. There is large number of extensive publications on these aspects available such as [9-13].

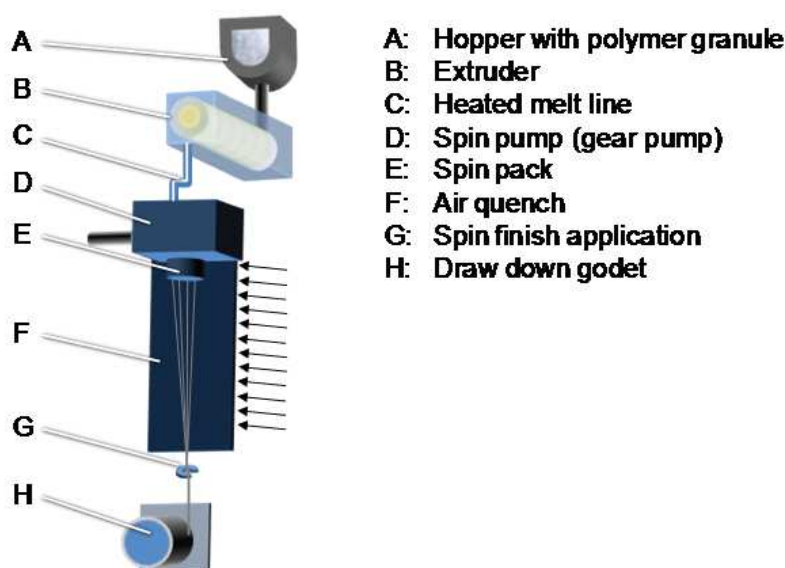


Figure 1. Schematic overview of a conventional melt spinning line

The cooling of the material from melt to ambient temperature takes place under tremendous stretching stress, which is characterized by the ratio between draw down and melt extrusion speed. This is commonly referred to as melt draw ratio (MDR). This melt draw ratio can vary between small one digit figures for rather thick filaments, e.g. fishing line applications, up to values well beyond 100 for fine filaments with diameters in the range of 1 to 50 μm . In most applications the fibers undergo a consecutive stretching or drawing stage after solidification. Thus this is called solid-state-drawing (SSD). Herein the filament is usually run between two rollers whereas the second roller is run at a higher speed than the first one. The speed ratio of the two rollers is referred to as the solid state draw ratio (SSDR) [2,11,12]. Usually, the solid-state-drawing is usually performed under elevated temperature levels.

This is usually realized by heated rollers, so that the fibers heat up before and after drawing when in contact with the surface of the rollers. Other principles can facilitate chamber ovens, contact heating plates or overheated steam. The process parameters of the drawing state also have a significant influence on the material structure, the orientation state and also the relaxation state. For example do fibers which are drawn and not properly heat-set a high degree of shrinkage which is usually unacceptable for most applications [2,4].

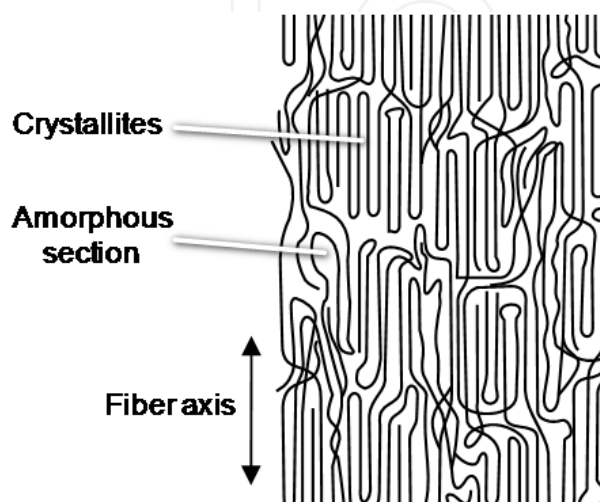


Figure 2. Model for the morphology in a polymeric fiber in allusion to [14]

In both cases the melt drawing as well as the solid state drawing the macromolecules are oriented along the fiber axis (see figure 2). This results in a unique morphology and crystalline structure which can be found only in fibrous materials in this highly oriented state [9,11]. Although there remains some controversy and vivid discussion about the resulting crystalline structure, scientist and researchers agree in the fact that the highly elongated material exhibits deformed crystallites as well as a highly ordered amorphous phase in the non crystalline regions.

For the description of the crystalline structure, most commonly the Stacked-Lamellae and the Shih-Kebab models are quoted [14]. This is usually based on small angle x-ray scattering data, which however do not provide a real image of the structure [15]. A closed theory about the development of the various morphologies is not available. For the thermo-dynamical description of the crystallization the Gibbs free energy is used [16]:

$$\Delta G_m = \Delta H - T \cdot \Delta S \quad (1)$$

Elongated states cannot be discussed within the equilibrium thermodynamics, because of the missing isotropic character of the morphology. Nonetheless, an adoption of the equilibrium theories through consideration of anisotropic influences in analogy to the electro-magnetic field theory is possible [16,17]. In literature [16] within the discussion of entropy elasticity it is described that elongation of a melt through an outside force results in an increase of the free energy of the material. Thus a deformation will result in an increased Gibbs energy ΔG_m in spinning and thus will significantly influence the crystallization of the polymer [16].

For the ideal Gaussian polymer chain this energy contribution corresponds with a reduction of entropy δS_{AL} in the elongated state [11]:

$$\Delta G_{m,AL} = \Delta H - T \cdot (\Delta S - \delta S_{AL}) \quad (2)$$

This change in entropy causes an increase of the crystallization temperature as well as an enhancement of crystallization rates. For polymorphic materials simple extensions of this theory are given in [18,19]. The different morphological phases are described through varying energy levels which depend on temperature and state of elongation and strain [19,20]. Depending on the process parameters and the material properties these phenomena are more or less prominent and detectable. Since the degree of crystallinity, the degree of orientation within the molecular structure and tendency of a material to crystallize when stored at temperatures above the glass transition temperature, thermal analysis is one key analytical method to investigate fiber materials, processes and fiber product properties.

2. Experimental method

The following text deals with the experimental investigation of polymeric materials. In this context the method of differential scanning calorimetry (DSC) is described and it will be pointed out what the general procedure is like and which experimental parameters have to be considered.

Differential scanning calorimetry follows the principle of the measurement of heat flow differences. By performing DSC a sample whose temperature is increased gradually and then subsequently cooled down is investigated and finally compared to a reference probe. Therefore it is possible to determine enthalpies and melting points of an arbitrary polymeric fiber. In this context a variation of the involved parameters offers a possibility to draw conclusions about underlying properties such as equilibrium values but concerning the execution of the experiment all of the possibly modifiable parameters have to be regarded carefully to perform DSC correctly. In order to perform DSC a furnace which can be heated up and cooled down homogeneously is required. Inside this oven there are two mountings for the samples and each mounting is equipped with a high-sensitive temperature sensor [21,23,24]. The general set up is depicted in figure 3.

One mounting (left mounting in figure 3) is for the crucible which contains the prepared sample. The lid of the crucible has at least one hole to allow an exchange with the surrounding atmosphere. Furthermore, pressure build-up in the crucibles is prevented if parts of the sample vaporize. The other mounting (right mounting in figure 3) is for an empty crucible which functions as a reference. Due to the usage of such a reference only effects caused by the sample itself are observable in the final thermogram. The oven is purged with a gas (sample gas), so that transitions and chemical reactions in different atmospheres can be examined. To avoid oxidation processes a protective gas (e.g. N₂ or Ar) can be used to create an atmosphere around the sample during the process of DSC. Otherwise, air or oxygen can be selected. Furthermore, the space around the oven is purged with a protective gas (N₂) to avoid ice formation at low temperatures [21-24].

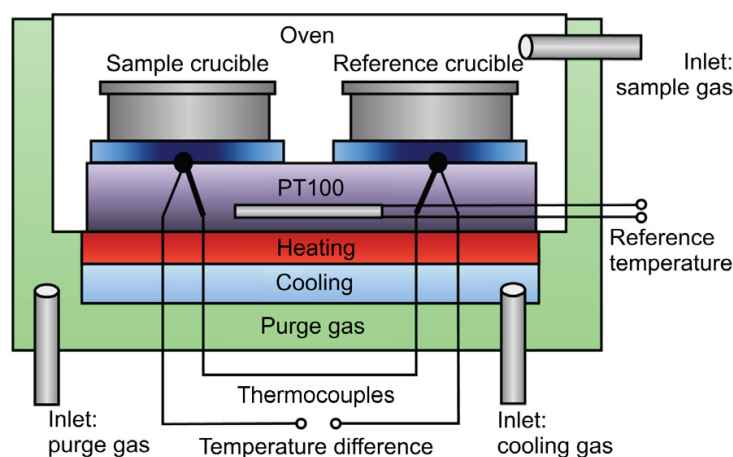


Figure 3. Schematic set up of differential scanning calorimetry

In a special form of differential scanning calorimetry a temperature-modulation is used. Usually one pre-defined frequency is used for temperature modulation [23,24]. The special TOPEM® (Mettler Toledo brand name) technique developed by Mettler Toledo allows the frequency-independent separation of reversing and non-reversing components of the heat flow by analyzing the impulse response of the sample to a pulse of stochastically varied length. Therefore a separation of overlapping effects is possible. Due to this separation extra insight can be gained [22].

3. Sample preparation

The process of sample preparation is of significant importance for the success of experimental investigation of polymeric fibers and has to be handled with great care. Additionally, different aspects of preparation have to be considered simultaneously in order to provide valid and reliable experimental results.

Before beginning with the experimental procedure itself, several aspects have to be dealt with. In general, both granules and fibers are treated in the same manner: The samples have to be reduced to small pieces so that they fit into the crucibles. In this context it is inevitably necessary to consider that the preparation method directly influences the results which are provided by differential scanning calorimetry. Therefore optimum conditions and parameters have to be found in order to determine certain effects (such as glass transition, crystallization or melting). Otherwise these effects still would be observable but not as good as if the optimum conditions were adjusted. Figure 4 conveys an idea which steps are necessary for sample preparation.

The sample has to be reduced to small pieces in order to perform the experiments. Therefore it is possible to alter the form and size of these pieces which yields different results. For example, the reduction to smaller pieces results in different observations concerning the gained thermogram. Usage of a sample with reduced size leads to a decrease of the peak and a lowered melting point. Therefore one can conclude that the mechanical aspect of preparation cannot be neglected and has to be treated carefully. Figures 5 a) and b) deliver an impression which mechanical appearance of the sample has to be chosen in the best case.

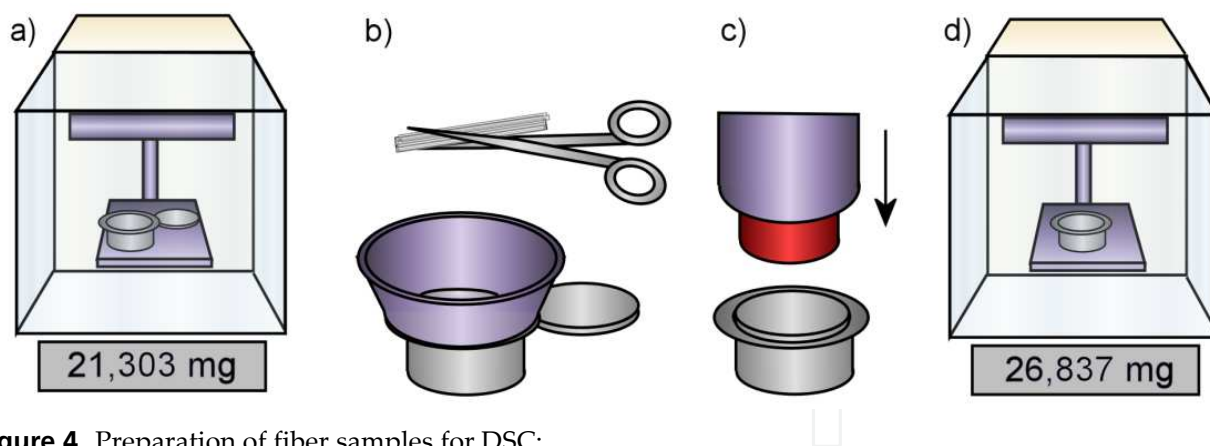


Figure 4. Preparation of fiber samples for DSC:
 a) Determination of the empty weight of the crucible
 b) Reduction of the fiber to small pieces
 c) Insertion of the crucible into cavity
 d) Determination of the total weight.

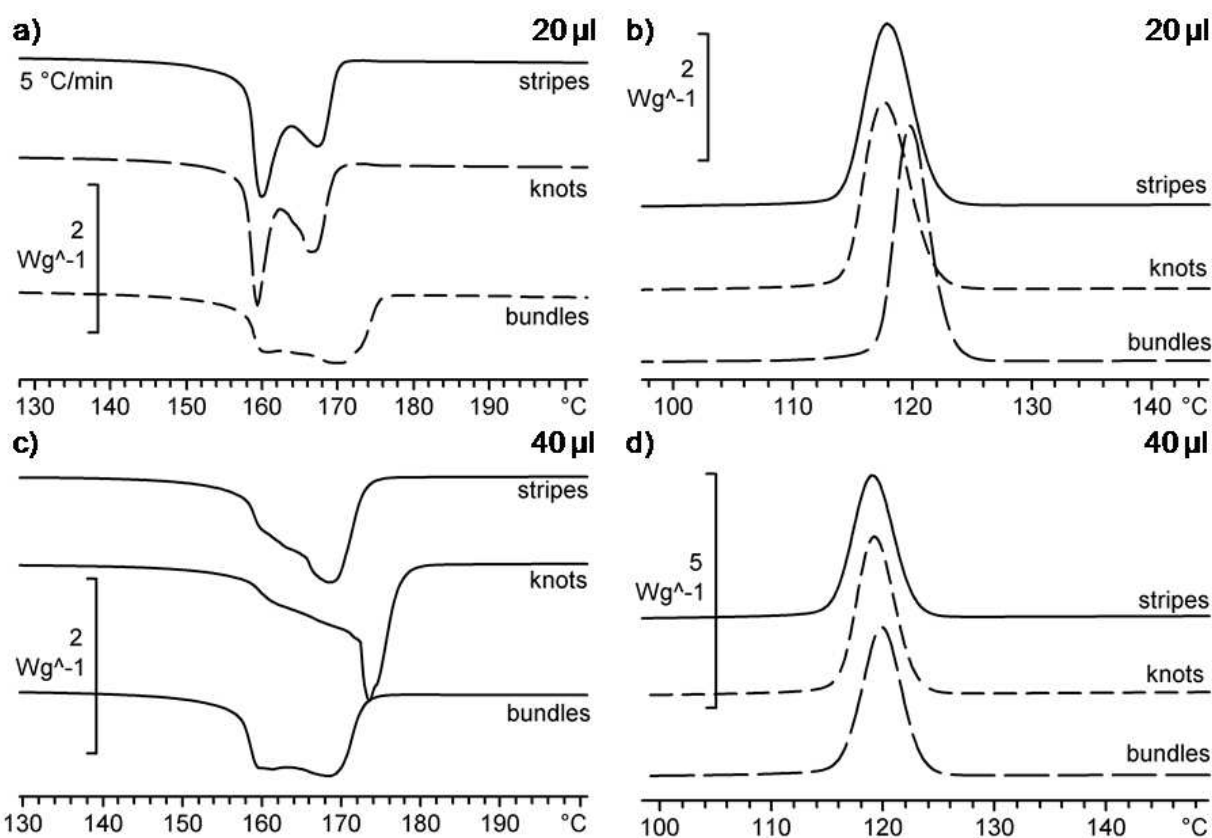


Figure 5. Effect of preparation conditions and crucible size
 a) Heating process with crucible volume of 20 μl ,
 b) Cooling process with crucible volume of 20 μl ,
 c) Heating process with crucible volume of 40 μl ,
 d) Cooling process with crucible volume of 40 μl .

Obviously, best results will be achieved if the sample is manufactured into short fiber chops (stripes). Especially knots cause irregularities as an unsteady graph in the thermogram. The

explanation for this phenomenon is that stripes offer an increased contact surface whereas knots melt discontinuously. Additionally, this result is independent on the volume of the crucible. In figures 5 c) and d) a similar thermogram is presented but the volume of the crucible is doubled (from 20 μL to 40 μL) and what is apparent here is the fact that again the short fiber chops provide the steadiest graph. Additionally, one can conclude that only the usage of the crucible with 20 μL volume delivers reliable results due to the fact that for the 40 μL crucible the graph inside the thermogram is rather uneven. This effect is caused by the better heat contact in the smaller crucibles, since the lid is pressed to the bottom of the crucible during the preparation process.

Concerning the weighted portion another remarkable effect can be observed: The peak height increases whereas the peak width drastically increases (see figure 6). Furthermore the onset temperature also increases logarithmically as a function of the sample mass. Nevertheless this result is rather obvious due to the fact that for the melting process of a sample with increased weight a higher amount of energy is required than for a sample with less weight. Concerning the interpretation of the results an advantage of less sample weight is that the peak sharpness is increased and therefore overlapping effects can be observed easier. In this context it is necessary to keep in mind that it is possible that thermal events that cause only little effects might be missed. These observations are depicted in the following diagram (figure 6), where the double peak during melting of polypropylene gets more separated for lower sample masses.

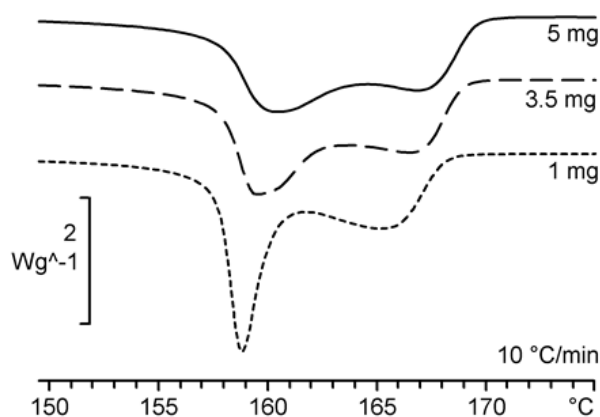


Figure 6. Normalized thermograms for different sample weight of polypropylene fibers

4. Influence of experimental parameters

To illustrate the effects caused by the variation of different parameters, several thermograms are shown in the following paragraph. All these thermograms refer to the investigation of fibers and as an example polypropylene (PP) was used. Firstly, the heating rate is varied as it is depicted in figure 7 a).

Analysis of the thermogram presented above conveys that the alteration of the heating rate causes a strong effect on the results delivered by differential scanning calorimetry. With all other parameters remaining constant the peak height and width increases with increasing

heating rate. Moreover, a double peak is of importance. Phase transitions only occur or can be separated from the melting process if lower heating rates are used. For high heating rates they cannot be observed.

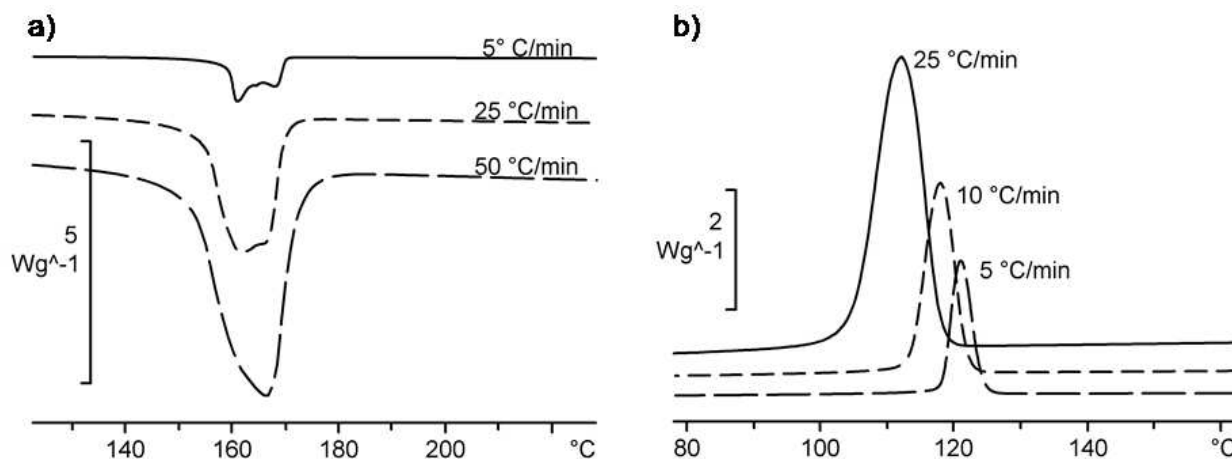


Figure 7. a) normalized thermograms for different heating rates for polypropylene fibers
b) normalized thermograms for different cooling rates of polypropylene granule

Secondly, the variation of the cooling rate is also important as it is depicted in figure 7 b). Beside other observations it is very obvious that the crystallization peak is shifted in positive temperature direction with decreasing cooling rates and the absolute height of the peak is also decreasing. Apparently the correct choice of the cooling rate is as important as it is for the heating rate for the analysis of crystallization processes. By taking into account different cooling rates and extrapolating the peak temperature to isothermal conditions (not measurable in DSC), the true crystallization point can be evaluated.

4.1. Fibers from commodity polymers

All results provided by the last paragraph yield that the alteration of heating and cooling rate causes a strong effect on the results of DSC. Due to this fact it is vital for the success of the analysis to consider the effect of the altering of especially those parameters mentioned above on the properties of a polymeric material which are in the center of interest. Among others the properties crystallization, melting and glass transition shall usually be investigated. In order to support the successful performance of DSC several hints and recommendations for various polymers will be presented in this paragraph. Typical commodity polymers are polypropylene (PP) [25], polyamide (PA6) [26] and polyethylene terephthalate (PET) [27]. In the following paragraph the effects of variations of heating and cooling rate on these polymers will be examined and presented.

Starting with PP (LyondellBasell Moplen HP561R [25]), in the following thermogram the results of DSC with different heating rates are depicted (figure 8 a)).

With increasing heating rate an increase of the peak height and width is noticeable. Additionally, the experiment's velocity is decreasing and the melting process starts earlier.

Noticeable is also the double peak when low heating rates were used. During the melting process of fibers it is likely that a phase transition from α - to γ -phase takes place [28]. The observation of this transition is depending on the choice of the heating rate because it is possible that the material melts directly or the effect is superimposed by others. Due to the fact that a characteristic amount of energy is necessary, it is possible to observe this transition as a peak in the thermogram if the heating rate is chosen correctly. After complete transition to γ -phase the sample will melt completely and another peak is observable in the thermogram. Now the distance between these mentioned peaks is depending on the heating rate and if this rate is adjusted inappropriately both effects are no longer separate from each other. Another possibility is that no phase transition occurs because the temperature is risen quickly enough to start the melting process directly.

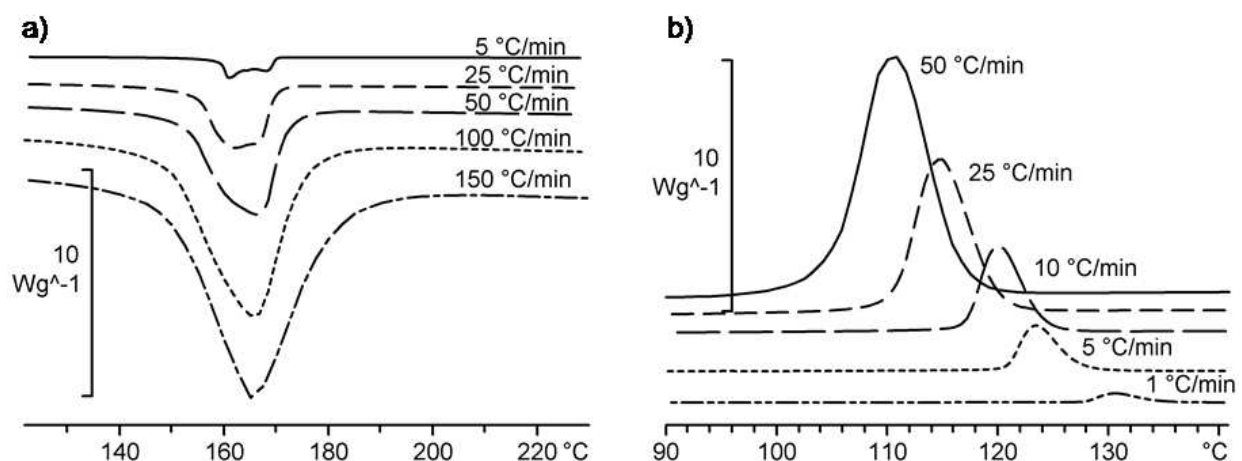


Figure 8. Normalized thermograms for different a) heating and b) cooling rates for PP

In the thermogram (figure 8 b)) the variation of the cooling rate is presented for PP. With increasing cooling rates the crystallization peak and its width increases. As reasonably expected the crystallization procedure is slower for higher cooling rates. The actual crystallization peak is determined by extrapolating a virtual crystallization peak for a heating rate of 0 °C/min from the peaks for known heating rates.

As the previous results were gained from investigations of PP similar experiments were performed for PA6 (BASF Ultramid B24N03 [26]). Beginning with a variation of the heating rate as it is depicted in figure 9 a).

Similar to PP the peak width and height is increased for higher heating rates. In this case another remarkable effect can be observed:

With heating rates higher than 25 °C/min a glass transition is starting below 50°C. This indicates that if heating rates below 25 °C/min were chosen this kinetic transition causes a too small effect and is therefore not visible. If the heating rate is then increased further another peak becomes observable. What is visible here is a phase transition from γ - to α -phase between 120 °C and 160°C [29]. For the observation of these two effects, it is therefore necessary to choose a heating rate above 25 °C/min.

In analogy the cooling rate is varied as it is depicted in figure 9 b). Similar to PP, the crystallization peak shifts to lower temperatures for higher heating rates and true crystallization point can be gained by an extrapolation of the peak temperature. The glass transition point cannot be observed since the actual state of the polymer chains is frozen in during cooling and changes in heat capacity will only be visible by heating up the sample again. Furthermore, the phase transition is also not visible since the material crystallizes in the α phase.

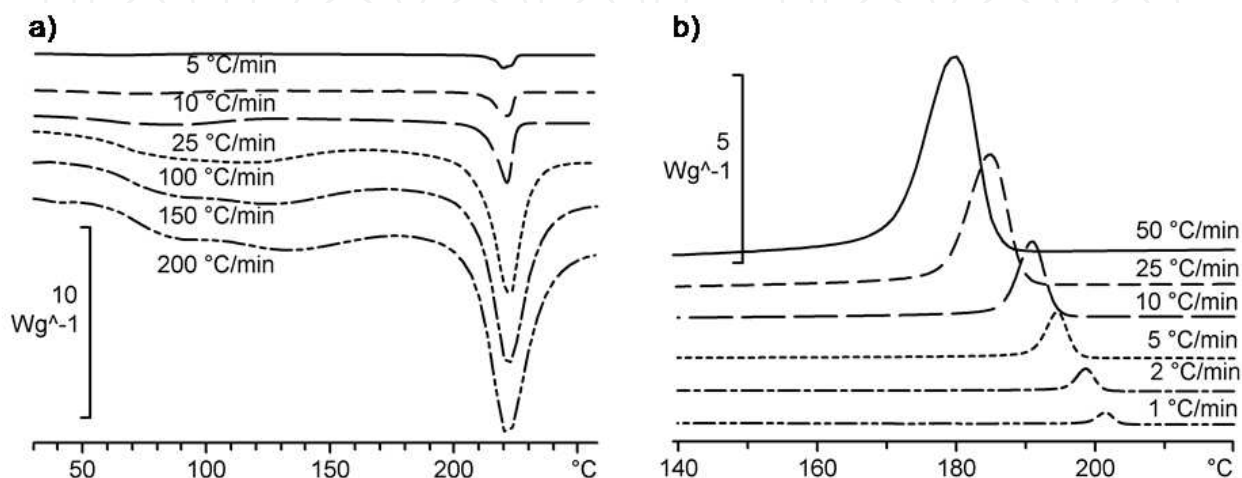


Figure 9. Normalized thermograms for different a) heating and b) cooling rates for PA6

Finally, DSC is performed for PET (Invista Polyester Chips 4048 [27]) and again heating and cooling rates are varied. Firstly, the heating rate is altered (figure 10 a)).

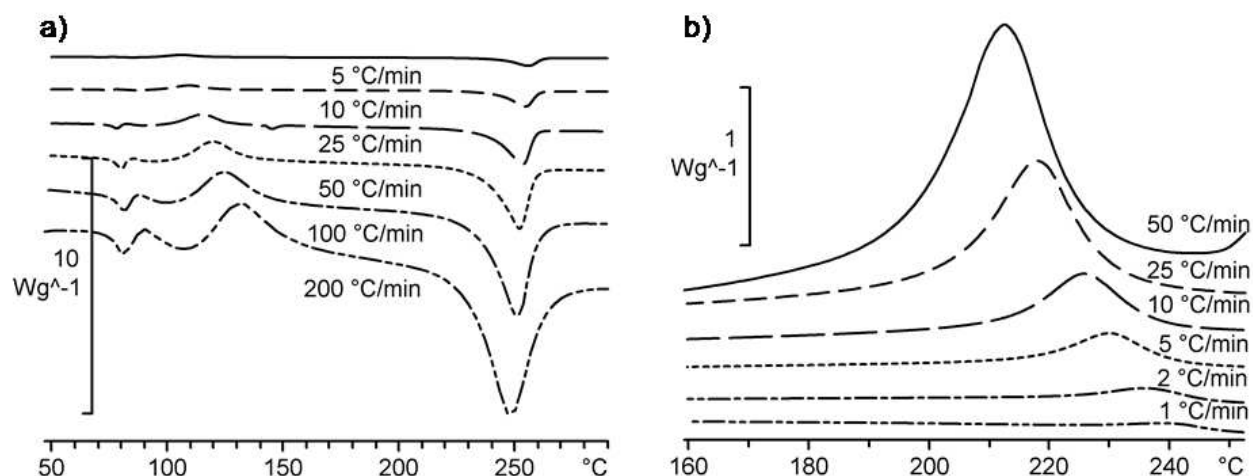


Figure 10. Normalized thermograms for different a) heating and b) cooling rates for PET

Again, the peak width and height increases with higher heating rates. But the glass transition is in this case even more remarkable: Beginning with a heating rate of 25 °C/min this transition becomes visible and is much more pronounced than it was in the investigation of PA6, since the mobilization of polymer chains during the transition has a larger influence on the heat capacity. Furthermore, a relaxation process can be observed

shortly after glass transition, indicating that the elongated state of the amorphous polymers chains was frozen in during the rapid cooling in the spinning process. At high heating rates another effect can be observed: after the glass transition and relaxation second crystallization occurs, which pronounces the quenching of the material during the spinning process. After heating over the glass transition point, the mobility of the amorphous or mesomorphous polymer chains increase so that the already present crystallites can grow.

Secondly, the cooling rate is changed for PET sample fibers (figure 10 b)). The analysis of this diagram yields similar results as for the investigation of PP and PA6. With increased cooling rates higher and broader crystallization peaks become visible. Additionally, these peaks are shifted to lower temperatures with increased cooling rates.

4.2. Recommendations

Using the results from the previous paragraph, one can conclude that the appropriate choice of heating and cooling rates is essential for the experiment's success. Therefore, the following table contains valuable information concerning the right choice of these rates in order to gain maximum benefit from performing differential scanning calorimetry of commodity polymers. In this context it is necessary to consider that with too high heating rates some effects may superimpose and therefore might not be visible.

Polymer	Process	Effect	Temperatures	Rates
PP	Heating	Phase transition ($\alpha \rightarrow \gamma$)	156 – 162 °C	< 25 °C/min
PP	Heating	Melting	162 – 170 °C	all
PP	Cooling	Crystallization	100 – 125 °C	all
PA6	Heating	Glass transition	50 – 60 °C	> 25 °C/min
PA6	Heating	Phase transition ($\gamma \rightarrow \alpha$)	100 – 170 °C	> 10 °C/min
PA6	Heating	Melting	200 – 240 °C	all
PA6	Cooling	Crystallization	160 – 200 °C	all
PET	Heating	Glass transition with relaxation	70 – 90 °C	> 25 °C/min
PET	Heating	Crystallization	90 – 160 °C	> 10 °C/min
PET	Heating	Melting	220 – 270 °C	all
PET	Cooling	Crystallization	190 °C – 240 °C	all

Table 1. Recommendations for the right choice of heating and cooling rates

5. Poly(vinylidene fluoride) fibers

Poly(vinylidene fluoride) is a thermoplastic, semicrystalline fluoropolymer with the monomer unit $[\text{CF}_2\text{-CH}_2]$. Due to the high fluorine content, it exhibits excellent chemical stability [30]. Furthermore, the polar side groups are responsible for the piezoelectric, pyroelectric and ferroelectric properties of the material, which are only present in one

crystalline phase of the polymorphic material, the so called β phase [31,32]. In total, four different crystalline phases can occur [33]. An overview of the crystalline phases, together with the conditions for their formation, is given in table 2.

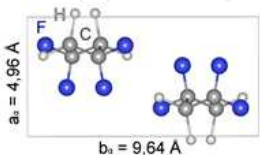
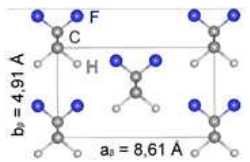
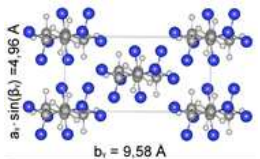
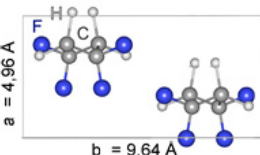
Crystalline phase	Molecular conformation	Crystalline unit cell (a-b-projection)	Polarity	Conditions for formation
α	TGTG'		non-polar	Cooled from melt, cast from solution
β	TT		polar (high)	Mechanical stress, high electric field
γ	TTTGTG'		non-polar	Heat treatment, cast from solution
δ	TGTG'		polar (low)	Electric field

Table 2. Crystalline phases of poly(vinylidene fluoride) [34-37]

If the material is present in the β phase, it can be used to create sensors or actuators, which are commonly used in the form of films in microphones, hydrophones or headphones. Here, the necessary process conditions (drawing of the films or high electric fields) for the β phase formation are well known [31,38].

In the case of fibers, the material could potentially be used as sensor or actuators. Possible applications include direction sensitive and spatially resolved strain measurement, which is useful for health monitoring in medical / smart textiles or structural health monitoring in fiber reinforced composites. However, suitable process conditions for fiber spinning, drawing and further processing steps have to be found, whereas β phase crystallites have to be formed and not be destroyed along the process chain [39-42]. Therefore, methods of thermal analysis were developed to identify the presence of the β phase, which are validated by additional X-ray diffraction measurements (WAXD) and dynamic mechanical analysis (DMA) [40,42]. In the following section of this chapter, these methods and their validation will be demonstrated, and they will be applied to gather information about phase transitions during melt spinning, drawing and heat treatment. Therefore, thermal analysis is a powerful tool for process analysis and the development of a process chain for the creation of piezoelectric sensor fibers.

6. Experimental details

Conventional and temperature modulated DSC are carried out on a DSC 1 from Mettler Toledo, Greifensee, Switzerland, equipped with a FRS5 sensor having 56 thermocouples. During the experiments, heating and cooling rates were varied between 1 °C/min and 20 °C/min in a temperature range between -90 °C and 250 °C, which corresponds to 50 °C below the glass transition and 70 °C above the melting point. As checked by thermogravimetric analysis, no weight loss and therefore no polymer degradation occurs in this temperature region during the relevant residence times. For the temperature modulated DSC analysis, TOPEM® technique by Mettler Toledo was used, where the constant heating rate was modulated with heat pulses of 0.5 °C height and stochastically varied length between 15 and 30 s (corresponds to 33.3 and 16.6 MHz). Experimental conditions for DSC analysis are summarized in table 3.

Parameter	Value	Unit
Starting temperature	-90	°C
End temperature	250	°C
Heating / cooling rate	1 / 2 / 5 / 10 / 20	°C/min
Constant heating / cooling rate (TOPEM®)	0.5 / 1 / 2	°C/min
Heat pulse height (TOPEM®)	0.5	°C
Heat pulse length (TOPEM®)	15 - 30	s
Crucible size (granule)	40	μl
Crucible size (fiber)	20	μl
Purge gas volume rate	50	ml/min

Table 3. Parameters for DSC experiments

Results of thermal analysis are compared to the polymer structure and polymer chain orientation, which are determined by wide angle x-ray diffraction (WAXD). Here, a 2D image plate system IPDS II from STOE & Cie GmbH, Darmstadt, Germany, is used for simultaneous analysis of structure and texture. Since the three most important crystalline forms of PVDF α , β and γ have unique diffraction patterns, the method can be easily used to identify the phases. By additional experiments with a heating chamber and heating rates similar to DSC, the underlying phase transitions can be assigned directly to their thermal effect. Since β phase formation can be achieved by mechanical stress, thermal properties of the material are further correlated to dynamic mechanical analysis (DMA), which is carried out on a DMA/SDTA861e by Mettler Toledo. Here, mechanical relaxation processes determined from the phase shift $\tan(\delta)$ between storage and loss modulus are correlated to their contributions to heat flow.

7. Properties of raw material

In this chapter, some information about the thermal properties and the crystallization behavior of the raw material (Solvay Solef® PVDF 1006 [43]) will be given, which can be

later on compared to changes in the fiber material. A typical DSC thermogram (with heating and cooling rate of 10 °C/min) of PVDF quiescently cooled from the melt (with a cooling rate of 1 °C/min) can be found in figure 11. As indicated in the figure, the melting and crystallization peak can be identified clearly.

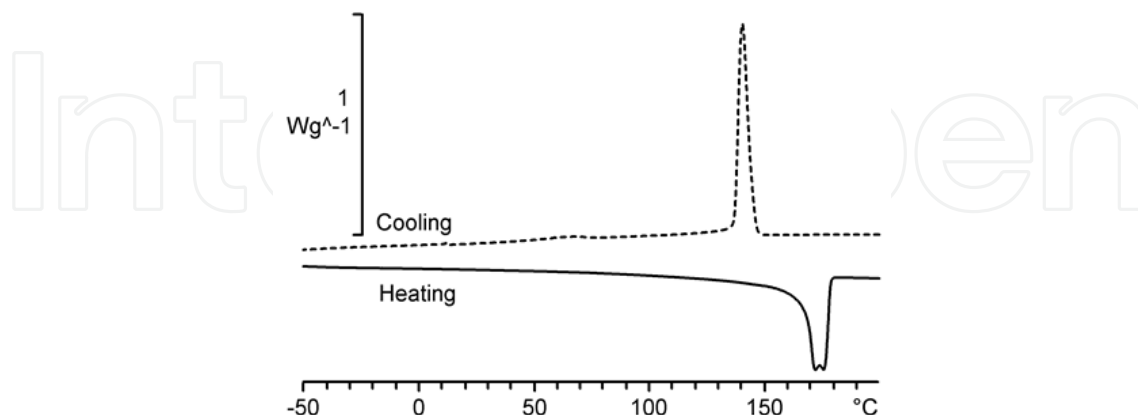


Figure 11. DSC thermogram (heating and cooling) for PVDF bulk material

The endothermal peak correlates to the melting of the material, which takes place in the temperature region between 165 and 180 °C. During the cooling phase, the crystallization (exothermal peak) takes place between 150 and 140 °C. When compared to X-ray data and polarizing microscopy, this behavior can be assigned to a non-textured α phase (figure 12 a), orientation factor $f = 0$) with spherulitic morphology (figure 12 b)). The material properties are summarized in table 4.

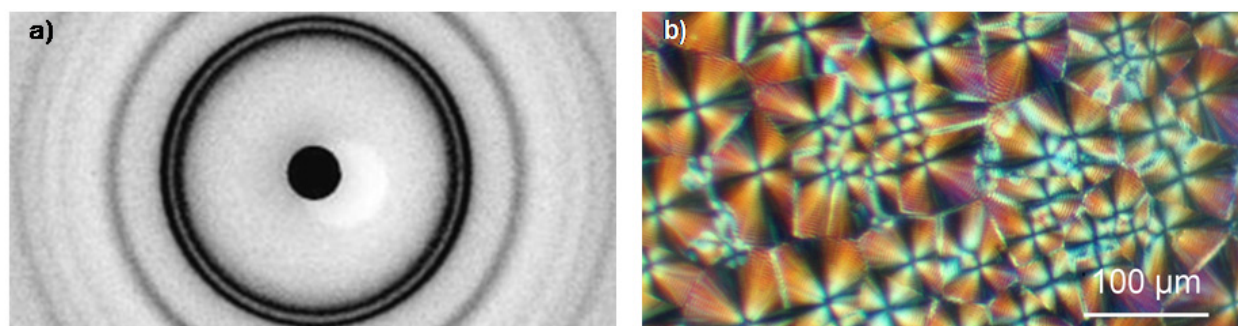


Figure 12. a) Diffraction pattern of quiescently cooled PVDF sample, b) Polarizing microscopy image of quiescently cooled PVDF sample.

8. Influence of the spinning process

PVDF fibers (multifilaments) are produced in an industrially relevant high speed spinning process. The winding speed is varied between 100 and 2500 m/min, which correlates to a melt draw ratio of 40 respectively 100. Due to this high draw ratios, polymer chains are oriented and orientation induced crystallization takes place. However, mechanical stress is relatively low during the melt drawing, so that the material crystallizes in a textured α phase (orientation factor $f \approx 1$). This information can be extracted from the X-ray data (figure 13 a)).

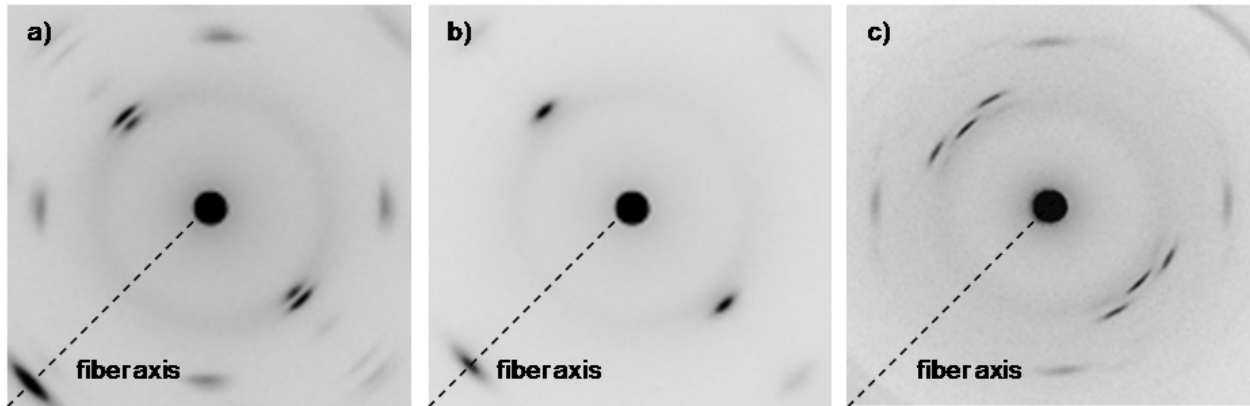


Figure 13. a) Diffraction pattern of melt spun PVDF fiber (winding speed 2.500 m/min),
b) Diffraction pattern of a drawn PVDF fiber (DR = 1.5, drawing $T_D = 140$ °C),
c) Diffraction pattern of a thermally treated PVDF fiber ($T = 165$ °C).

Depending on the heating rate, the melting behavior changes in the fiber material. After the melting peak, a second peak occurs (figure 14 a)). By further analysis (section “phase transitions during heat treatment”), this peak correlates to the melting of the γ phase, which is converted from α phase during the heating process. This peak gets larger for lower heating rates, since the process of γ phase conversion has more time to take place. Further evidence for changes in this kinetics can be found in the shape of the melting peak, whereas the first part of the peak becomes larger for lower heating rates. Furthermore, γ phase formation is more promoted in fibers produced with higher winding speeds (figure 14 b)). Here, also the same effect on the melting peak (shift to the first part) can be found.

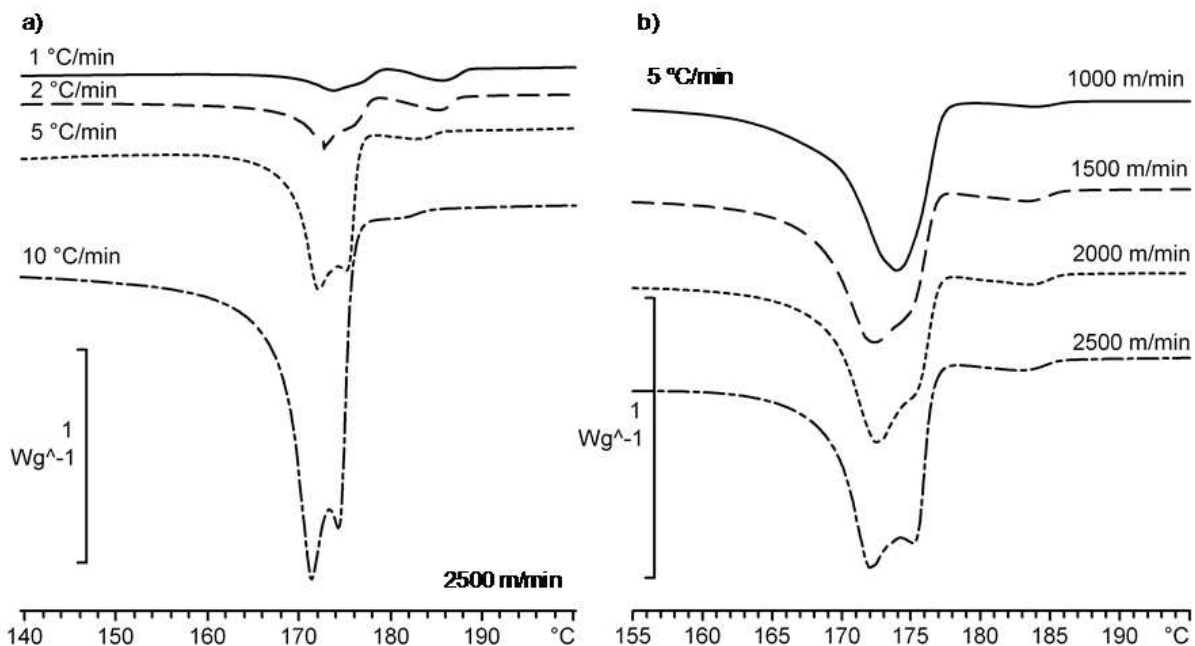


Figure 14. Melting behavior of melt spun PVDF fibers:

- a) as a function of the heating rate,
- b) as a function of the take up velocity.

Typical values for thermal and structural properties for a melt spun fiber can be found in table 4. Even though the material is cooled down with about 1.000.000 °C/min during fiber spinning, the melting enthalpy is exactly in the same range compared to the slowly cooled sample. This emphasizes the strong enhancement of crystallization rates due to the uniaxial orientation in the spinning process.

9. Influence of the drawing process

In the drawing process, a plastic deformation of the material in the solid state takes place, whereas the drawing ratio DR and drawing temperature T_D can be varied. Starting from the standard process (DR = 1.4, T_D = 140 °C), drawing ratio and temperature are varied separately between 1.0 and 1.6 as well as 40 °C and 160 °C respectively. The effect of both parameters on the melting behavior is displayed in figure 15.

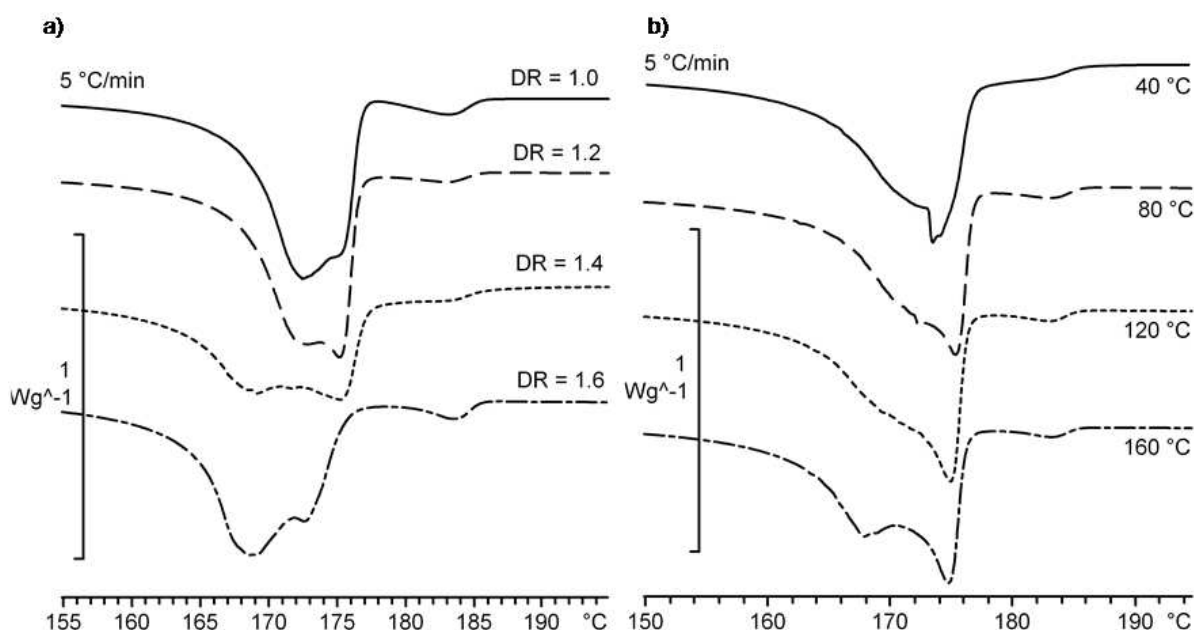


Figure 15. a) Changes in the melting peak as a function of draw ratio,
b) Changes in the melting peak as a function of drawing temperature.

A main effect of the drawing process is a modification of the melting peak, whereas peak temperature shifts to lower temperatures with higher drawing ratios (168 °C for the highest draw ratio compared to 173 °C for an as-spun fiber). In the X-ray diffraction pattern (figure 13 b)), the formation of β phase can be identified, so that the modification of the melting peak correlates to this crystalline phase. Like in the undrawn fiber, the peak coming from γ phase melting can also be found. The same effect can be found by increasing the drawing temperature. The underlying phase transitions during the melting process will be described in detail in the next section. At lower temperature regions, further peaks can be found (figure 16) depending on the drawing temperature. For low temperatures, a signature close after the glass transition point (-35 °C) can be found. A second peak can be found at higher temperatures, which is present in all fibers. For undrawn fibers, the peak temperature is around 55 °C and for drawn fibers about 5 °C higher.

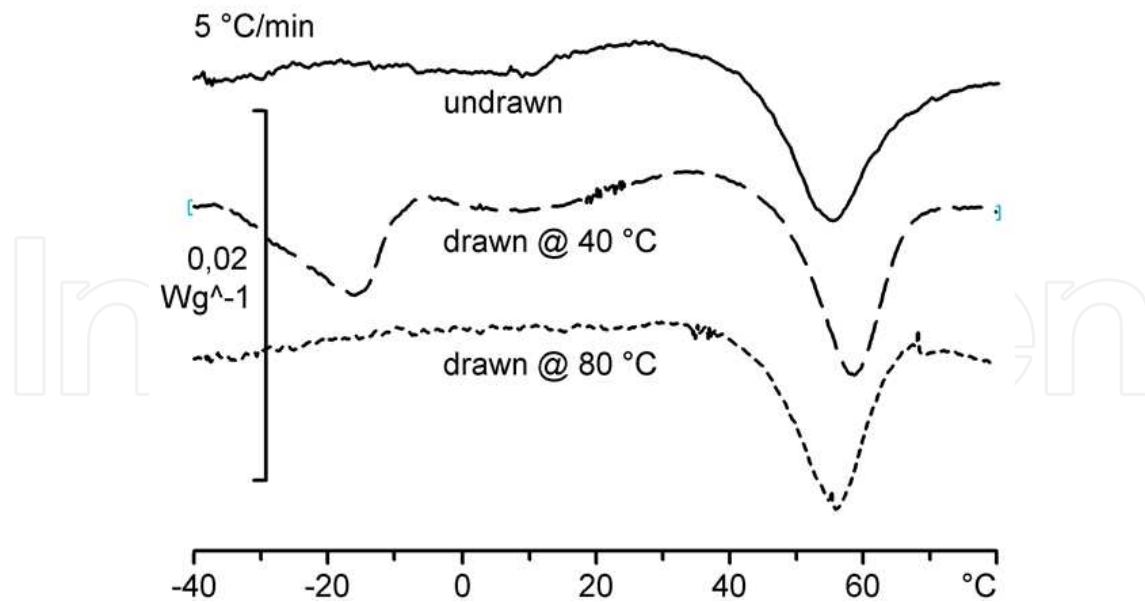


Figure 16. Relaxation processes at different drawing temperatures (draw ratio DR = 1.4)

Both peaks correlate a relaxation process, which can be found in DMA measurements, which are displayed in figure 17. Here, glass transitions can be identified easily. Another relaxation process (known as α_c relaxation in other types of polymers [44]) can be found at 55 °C (α phase) and at 60 °C (β phase), so there is clear evidence for a heat contribution to DSC measurements of this relaxation process. A reason for the occurrence of the first peak in coldly drawn fibers is a drawing temperature below the relaxation temperature, so that more energy is stored in the material and released when heated above glass transition temperature.

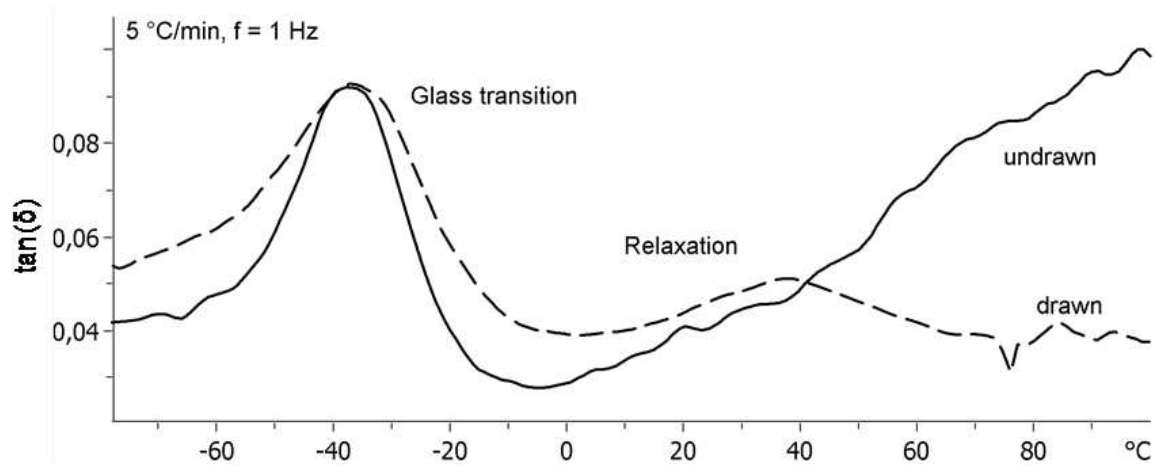


Figure 17. Phase shift $\tan(\delta)$ in dynamic mechanical response of the material

When compared to X-ray diffraction measurements, β phase amount is drastically increased without affecting overall crystallinity if the fibers are drawn above the relaxation temperature. Therefore, the relaxation process takes place in the α phase and promotes β phase formation. The properties of all fibers are summarized in the table 4.

Parameter	Value	Value	Value	Unit
Type of material	Granules	Melt spun fiber	Drawn fiber	-
Relaxation temperature range	-	36 - 65	40 - 71	°C
Relaxation temperature peak	-	55	60	°C
Relaxation enthalpy	-	1.6	1.3	J/g
Melting range	168 - 180	168 - 185	165 - 185	°C
Melting peak temperature	174	173	168	°C
Melting enthalpy	49.6	48.2	45.8	J/g
Crystallization range	140 - 150	_*	_*	°C
Crystallization peak temperature	145	_*	_*	°C
Crystallization enthalpy	50.0	_*	_*	J/g
Crystalline phase	α	α	β	-
Morphology	spherulitic / non-textured	textured	textured	-

Table 4. Thermal and structural properties of PVDF (*: not detectable since determined by process)

10. Phase transitions during heat treatment

Heat treatment is important in the further processing of the fibers. If they are to be used as piezoelectric sensors, a polarization process has to take place at elevated temperatures without having a reversion of β phase to α phase. To identify such a transition and explain phase transformations during the melting procedure of the material, temperature modulated measurements can be used. However, the occurrence of different crystalline phases has to be validated X-ray measurements of heated fibers. The results for temperature modulated measurements (TOPEM ®) are displayed in figure 18 for a undrawn and a highly drawn fiber, whereas heat flow is separated into reversing and non-reversing parts.

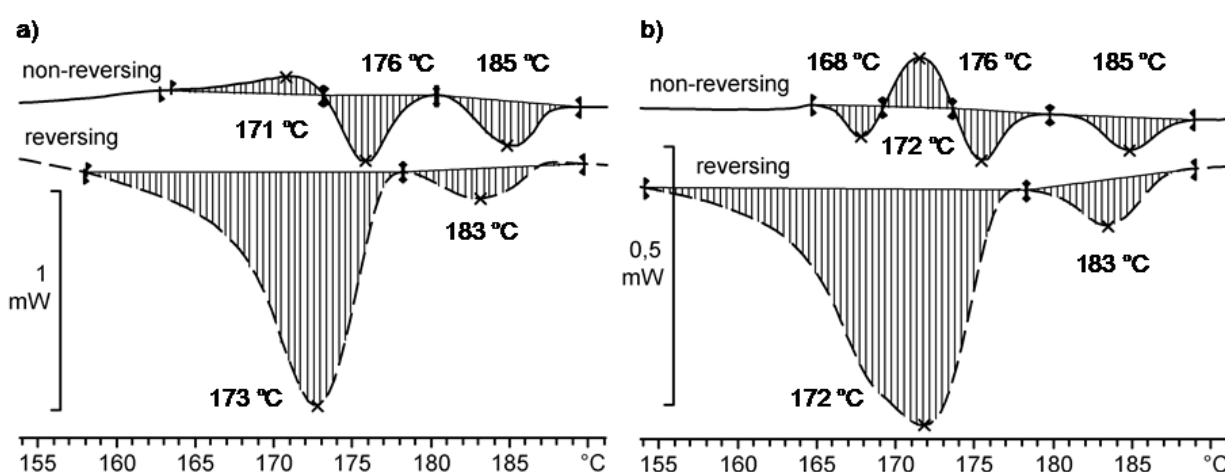


Figure 18. TOPEM ® results with constant heating rate of 2 °C/min (melting peak):

- a) PVDF fiber containing α phase,
- b) PVDF fiber containing β phase.

For an interpretation of the results, the highly oriented crystalline structures have to be taken into account. They were formed far from equilibrium and therefore must contribute to the non-reversing heat flow. On the other side, energy stored in the solidified amorphous parts due to short-range bonding to neighbor polymer chains contributes to the reversing heat flow. However, also crystalline phases contribute to the reversing heat flow if time scale of the phase transitions is larger than the pulse length applied to the sample. In total, 3 (α phase fiber) or 4 (β phase fiber) transformations in the crystalline regions take place. The same amount of phase transitions can also be found in X-ray measurements. The additional peak in the β phase fibers is caused by a reversion to the α phase. After this transition, the changes in the crystalline structure are the same for both fibers, starting from α phase conversion to γ phase, going on with the melting of the remaining α crystallites and finally ending with the melting of the γ phase. Since the melting of the α phase takes place shortly after the conversion to γ phase, the amount of γ phase (compare to figure 14) strongly depends on the heating rate. All phase transitions during heat treatment are summarized in table 5.

Transition	Temperature range (peak)	Heat flow
$\beta \rightarrow \alpha$	165 °C – 170 °C (168 °C)	endothermal
$\alpha \rightarrow \gamma$	166 °C – 173 °C (171 °C)	exothermal
$\alpha \rightarrow \text{melt}$	173 °C – 180 °C (176 °C)	endothermal
$\gamma \rightarrow \text{melt}$	180 °C – 190 °C (185 °C)	endothermal

Table 5. Summary of phase transitions in PVDF fibers during heat treatment

11. Overview over phase transitions

For the selection of the right process settings for the production of piezoelectric fibers, it is necessary to get an overview of all phase transitions which can occur in the processes (melt spinning, solid state drawing and heat treatment/polarization). All these transitions were described in the previous sections and are summarized in figure 19.

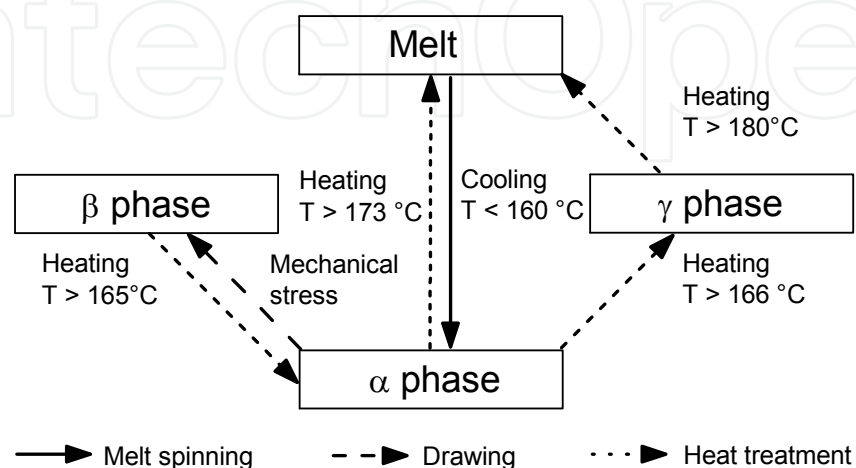


Figure 19. Overview of phase transitions in poly(vinylidene fluoride) fibers

After melt spinning, the fibers should be drawn at high ratios (close to maximum elongation) to form as much β phase fraction as possible. Drawing temperature should be at least above 55 °C to enhance β phase formation and prevent relaxation processes. For further polarization processes, temperature should be kept below 160 °C to keep the material in the β phase. For the process development, calorimetric measurements are of great value to identify the phase transitions, so that they can be realized in the process by choosing the right parameters. Furthermore, thermal analysis is of great value for further quality control, since the present crystalline phases can be detected by a simple method (compared to techniques like X-ray diffraction).

12. Carbon nanotube composite fibers

Carbon nanotubes (CNT) are allotropes of pure carbon in a form of a cylindrical structure. Depending on the number of graphite sheets forming the tube, they are divided into single wall (SW-CNT) and multi wall carbon nanotubes (MW-CNT). Beside excellent mechanical properties, CNT offer high electrical and thermal conductivity. When added to a polymer matrix, their properties are partially transferred to the polymer nanocomposite material [45]. In the case of mechanical reinforcement, an increase of Young's modulus can be observed in many polymer matrices [45,46]. One of the most interesting aspects is the formation of electrical conductive paths, so called percolative networks, in otherwise insulating materials [45,47]. Compared to other conductive fillers like carbon black (CB), the amount of CNT for reaching electrical conductivity is extremely low, whereas percolation thresholds below 0.1 % were observed [48].

However, not only the desired material properties in solid state change by the additivation of CNT. The nanoparticles interact with the polymer matrix and influence the rheological properties of the polymer melt, but also the crystallization behavior [46]. Especially in the melt spinning process, process settings have to be adjusted to allow the production of CNT modified nanocomposite fibers [49-53]. Therefore, the nanocomposites have to be analyzed by DSC to understand the effects of CNT on the different polymer matrices, so that the right process parameters for fiber production can be found. Furthermore, thermal analysis provides useful information about the functional properties of the material, since crystallization conditions have a large influence on the electrical conductivity.

13. Experimental conditions

For each polymer, conventional DSC was carried out at least 50 °C below the glass transition (except of polyethylene, where glass transition is too low) and 50 °C above the melting point. Heating rate was varied between 2 °C and 20 °C, whereas results with 5 °C/min are shown in this chapter, since all effects to be demonstrated can be found at this heating rate.

Electrical properties of the composite materials were checked with a LCR meter, whereas the materials were tested in a frequency range between 1 Hz and 100 kHz. By checking AC conductivity, effects of partially not connected conductive networks can be found.

Furthermore, the values determined at low frequencies can be considered as the DC conductivity of the material.

14. Compounding in different polymer matrices

Depending on the type of polymer, CNT can influence the crystallization process in two different ways. Both effects will be described in this section with the help of the examples polypropylene (PP, Basell Moplen HP561R [25]) and polyamide 6 (PA6, BASF B24N03 [26]).

In PP (compare figure 20 a)), crystallization peak shifts to higher temperatures with increasing amount of CNT. This effect has two reasons. First, the high thermal conductivity of CNT allows the latent heat to be transferred faster from the polymer to the surrounding medium, so that sample temperature is closer to the reference temperature compared to unmodified samples. However, this effect shifts the peak only about 0.5 °C per w% CNT added to the polymer. The more dominant effect is the acting of CNT as foreign substance in the polymer, on which crystal nuclei can be formed at higher temperatures. After this nucleation, crystallites can grow in the usual way. By adding only 1 w% of CNT, this effect shifts the melting peak by 5 °C to higher temperatures.

The effect in PA6 is different (see figure 20 b)). The form of the crystallization peak changes to that a double peak can be found. Here, the part of the peak at lower temperatures (which is also shifted compared to unmodified material), has the same origin like in PP. Here also higher crystallization temperature is caused by enhanced thermal conductivity and crystal nucleation on the CNT. The part of the peak at higher temperatures is caused by another effect, the direct crystal growth on the CNT. The particles act as nuclei for the polymer chains and the crystallites can grow at higher temperatures, since no undercooling is needed for crystal growth compared to nucleation.

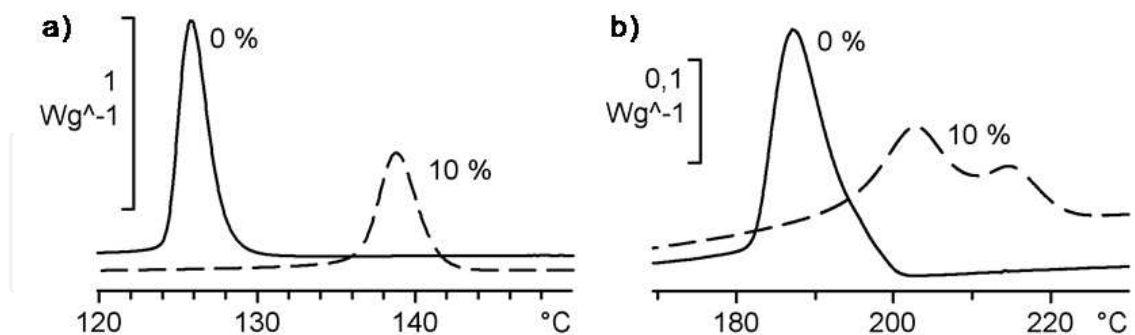


Figure 20. Effect of CNT on polymer crystallization (cooling rate 10 °C/min):

a) Polypropylene (PP),

b) Polyamide 6 (PA6).

The type of crystallization process has a large influence on the electrical properties of the material, especially on the percolation threshold. A comparison of the electrical properties of the two polymers can be found in figure 21 a). The percolation threshold is the value for CNT concentration, where the specific resistivity drastically decreases over several orders of magnitude. Above the threshold, resistivity only decreases slowly due to the higher amount

of conductive filler. For polypropylene, the threshold can be found at 3 w% compared to 7 w% for polyamide 6.

For polypropylene, CNT act as nucleation seeds, but the material has no chemical affinity to the nanoparticles. Therefore CNT try to form aggregates in the polymer matrix, which can build conductive paths through the whole fiber. The region between the aggregates is then filled by PP crystallites during the crystallization process. Because of the separation of the different regions, only lower amount of CNT is needed to form conductive paths. Therefore, the dynamic percolation threshold defined by the crystallization process is significantly lower than it would be for a uniform distribution of the particles in the fiber. This behavior can be observed with transmission electron microscopy (figure 21 b)).

For polyamide 6, where polymer crystallites directly grow on the particles, a chemical affinity between the components is given and single CNT are separated by the polymer matrix (see figure 21 c)). Therefore, CNT are well distributed in the polymer and the percolation threshold is defined by the geometry of the nanoparticles (length and diameter) as well as their orientation to the fiber matrix. Single CNT in PA6 can be oriented better compared to the aggregates in PP, so that the resistivity of a fiber is highly sensitive to the process parameters in the spinning and drawing process.

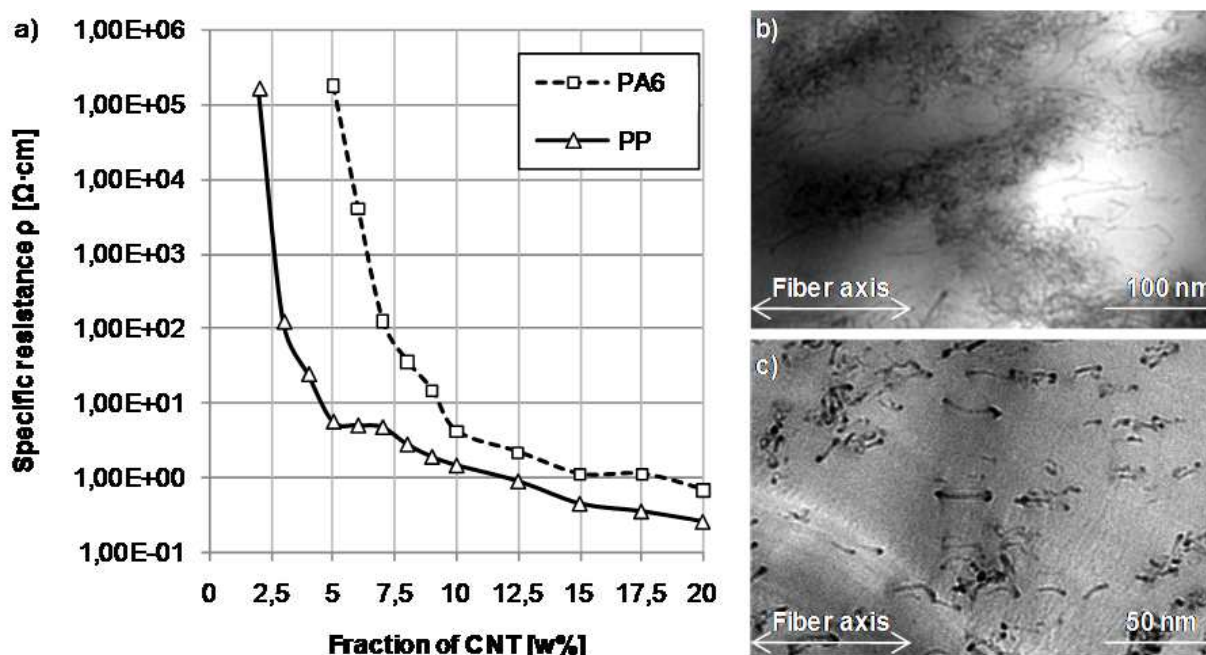


Figure 21. a) Electrical conductivity as a function of CNT weight fraction in different polymer matrices (PP and PA6),
 b) Transmission electron microscopy image of 10 w% CNT in PP,
 c) Transmission electron microscopy image of 5 w% CNT in PA6.

15. Influence of the spinning process

As described above, CNT have a major influence on the crystallization behavior in the different polymers. Even though the material is cooled down much faster during melt spinning and orientation induced crystallization is dominating the structure formation in the material, crystallization phenomena are drastically altered due to the presence of the nanoparticles. An example for the changes in the crystallization of polypropylene can be found in figure 22. If the material is heated above the relaxation point (approx. 50 °C), recrystallization phenomena can be found in the unmodified fibers. If CNT are doped to the PP matrix, no recrystallization peak can be found. Since the melting enthalpy is constant for different CNT fractions compared to the raw material (after recrystallization), it can be concluded that crystallization rates are enhanced by the presence of the particles. This observation is correlating with the fact, that the material cannot be drawn at high ratios in the molten state if CNT are present.

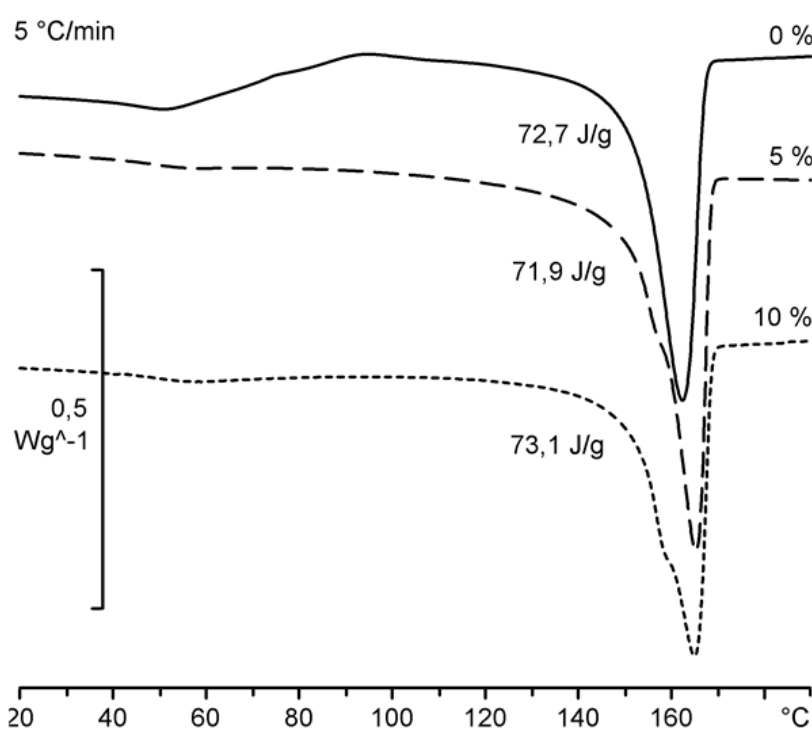


Figure 22. Changes in the melting behavior as a function of CNT concentration in polypropylene fibers spun with a winding speed of 50 m/min

In polyamide 6, the thermal property affected mostly is the glass transition. This effect is displayed in figure 23. By adding higher amounts of CNT, the glass transition temperature shifts to higher values. Thus a T_g of 60 °C is reached for a concentration of 10 w% compared to 52 °C for the same type of unmodified material. Since polymer crystallites grow on the CNT surface, the material is the polymer matrix has a better chemical bonding to the nanoparticles and the polymer chain mobility is lowered due to their presence. Therefore, more energy is needed to mobilize the polymer chains resulting in a higher glass transition temperature.

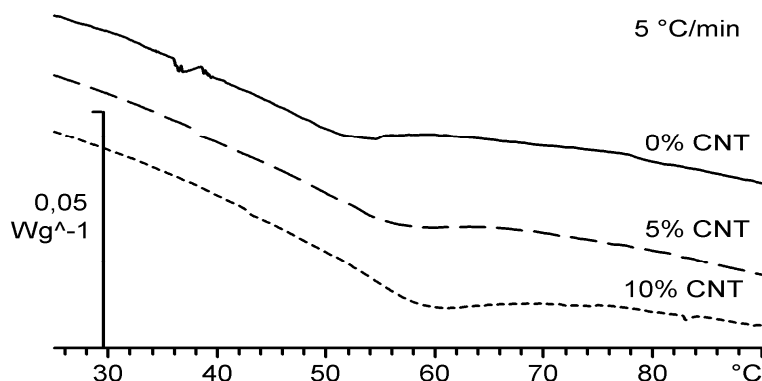


Figure 23. Changes in the glass transition as a function of CNT concentration in polyamide 6 fibers spun with a winding speed of 50 m/min

16. Effects in blend systems

In blend systems, two or more polymers are mixed together without forming a mutual polymer chain. If both components are not compatible with each other, they are separated in the fiber material, but influence each other [54]. Depending on the chemical structure of the polymers, CNT are attracted more by one of the components and aggregate in this material. This effect will be explained on a mixture of polypropylene (PP, LyondellBasell Moplen HP561R [25]) and low-density polyethylene (LDPE, LyondellBasell Lupolen 1800S [55]). The crystallization and melting behavior can be found in figure 24. In the crystallization process, the PP peak shifts by the additivation of CNT, which indicates the nucleation of PP

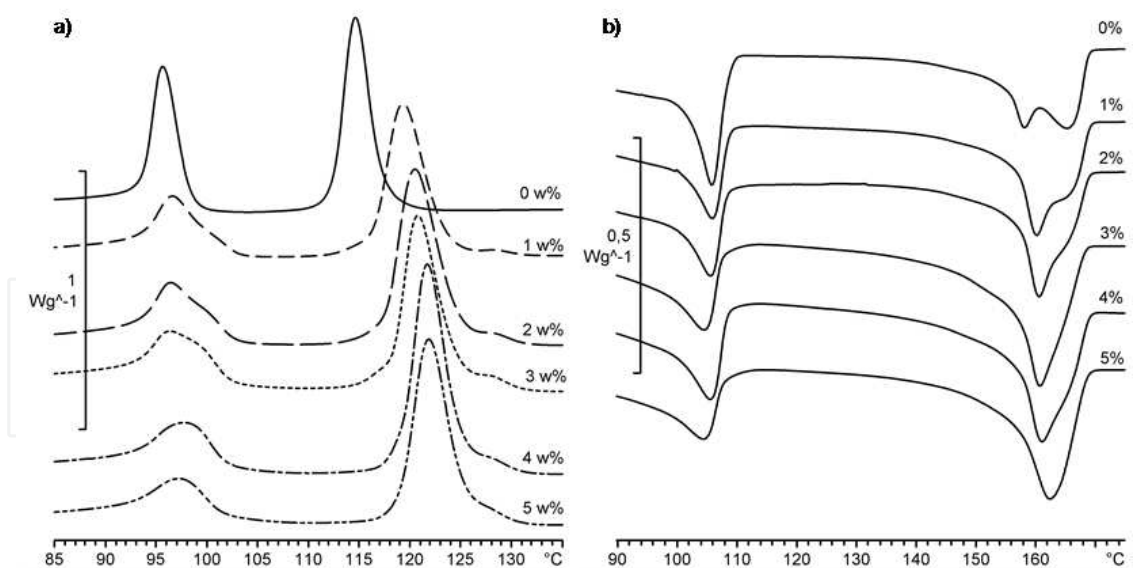


Figure 24. Effect in blend systems of polypropylene / polyethylene (1:1, heating/coolingrate 5 °C/min) as a function of CNT concentration:

- a) Crystallization phenomena during cooling of bulk material,
- b) Melting phenomena during heating of fibers.

on the CNT and therefore the presence of nanotubes in this polymer. For LDPE, there is no temperature shift of the crystallization peak. However, the peak gets broader. This indicates

major changes in the phase separation behavior, but without changing the crystallization process by the nanotubes. Possible reasons for the broadening are more diverse sizes of regions of LDPE in PP, which tend to crystallize at different temperatures. Further evidence of the aggregation of CNT in PP can be found in the melting process. While the form of melting peak of LDPE is not changed at all, the PP changes from a double peak to a single peak. Since the occurrence of the double peak indicates a phase transformation before the actual melting procedure, it can be concluded that the present crystalline phase (α phase) is stabilized by the presence of CNT and the nanotubes are situated in the PP phase of the blend system.

17. Impact on the development of electrically conductive fibers

As stated above, the choice of the base polymer as well as the melt spinning of the fibers has a large influence on the electrical conductivity. The base materials can be classified into two groups. In polymers like polypropylene, CNT act as nucleation seeds. The particles can aggregate and easily form conductive paths, so that a low percolation threshold can be observed. This class of materials is very useful for the production of electrically conductive fibers with high spinning speeds, since electrical conductivity is less affected by the spinning process and possible mechanical treatment during the use of the fibers. For polymers like polyamide 6, crystallites grow on the surface of CNT, so that particles are separated and the percolation threshold is higher. Since single CNT can be oriented easily, the spinning and drawing process has a larger influence on the conductivity. This makes the processing of the materials more instable. However, they can potentially be used to create sensors, whereas mechanical stress and deformation can be detected by changes in the resistivity.

18. Conclusion

Taking into account the unique morphology of polymeric fibers, special analysis methods are needed for the development of new materials and processes. Due to high deformation of the molten polymer in the spinning process as well as the solid-state deformation during drawing, the polymer chains are highly oriented along the fiber axis. Differential scanning calorimetry, especially with temperature modulation, is one of the most important tools for fiber development. It can be used for a fundamental study of new materials and their behavior during spinning and processing as well as quality control of commodity polymers.

For the analysis of commodity polymers, the effect of sample preparation and experimental parameters is demonstrated. For the preparation of samples, small crucibles with fibers cut into small pieces are useful to measure thermograms with clearly visible effects. The choice of parameters has a large influence on the thermal effects observable in the results. Depending on the heating and cooling rate, effects like glass transition, structural phase transitions, melting and crystallization can be revealed from the thermograms. For the observation of these effects in the most common fiber polymers (polypropylene, polyamide 6 and poly(ethylene terephthalate)), recommendations for experimental parameters are given and the temperature ranges for these effects are indicated.

The development of new spinning processes is demonstrated for poly(vinylidene fluoride), whereas DSC can be used to detect the formation of the piezoelectric β phase. With the help of temperature modulated DSC compared to X-ray diffraction and dynamic mechanical analysis, a process chain for the generation of piezoelectric sensor fibers with possible spinning and drawing parameters was developed. Since the formation of the piezoelectric crystallites can be detected by DSC, it is a powerful tool for future development of piezoelectric sensors and actuators.

Electrically conductive nanocomposites based on carbon nanotubes are used as an example for the development of new materials. The presence of nanoparticles influences the crystallization process dependent on the chemical structure of the polymer matrix, whereas two different mechanisms can be detected. The resulting structure then determines the percolation threshold for electrical conductivity. If polymer crystallites can directly grow on the CNT, the particles are separated and percolation threshold is only determined by the particle geometry and orientation. In the other case, the affinity of the polymer chains to the CNT is lower, so that they act as nucleation seeds. CNT can then aggregate and form conductive paths. Due to the higher separation of the two components, percolation threshold is lower.

Author details

W. Steinmann*, S. Walter, M. Beckers, G. Seide and T. Gries
*Institut für Textiltechnik (ITA) der RWTH Aachen University,
Aachen, Germany*

Acknowledgement

Special thanks to the Deutsche Forschungsgemeinschaft (German research foundation, DFG) for funding the project GR 1311/10-2.

19. References

- [1] Engelhardt A (2011) Global synthetic industrial filament yarn and fiber markets. *Chemical Fibers International*. j. 61: 122.
- [2] Fourné F (1995) *Synthetische Fasern: Herstellung, Maschinen und Apparate, Eigenschaften; Handbuch für Anlagenplanung, Maschinenkonstruktion und Betrieb*. München: Hanser. 880 p.
- [3] Gries T, Sattler H (2005) *Chemiefasern*. In: Winnacker K, Küchler L, editors. *Chemische Technik*. Weinheim: Wiley
- [4] Wulfhorst B, Gries T, Veit D (2006) *Textile Technology*. München: Hanser. 320 p.

* Corresponding Author

- [5] Walter S, Steinmann W, Gries T, Seide G, Schenuit H, Roth G (2010) Production of textile fabrics from PVDF multifilament yarns with textile titer. *Technical Textiles*. j. 53: E95-E97.
- [6] Walter S, Steinmann W, Gries T, Roth G, Seide G, Schenuit H. Tools for savers of life : production of warp-knitted fabrics from PVDF multifilament yarns of textile fineness. *Kettenwirk-Praxis*. j. 45: 34-36.
- [7] Walter S, Steinmann W, Seide G, Gries T, Roth G (2012) Development of innovative fibre materials for technical applications : fine polyvinylidene fluoride filaments and fabrics. *Filtration*. j. 12: 60-64.
- [8] Michaeli W (2010) Einführung in die Kunststoffverarbeitung. München: Hanser. 256 p.
- [9] Ziabicki A (1976) Fundamentals of fiber formation. London: Wiley. 504 p.
- [10] Ziabicki A, Kawai H (1985) High-Speed Fiber Spinning – Science and Engineering Aspects. London: Wiley. 586 p.
- [11] Salem D (2000) Structure formation in polymeric fibers. München: Hanser. 578 p.
- [12] Beyreuther R, Brüning H (2007) Dynamics of fibre formation and processing. Berlin: Springer. 365 p.
- [13] Nakajima T (1994) Advanced fiber spinning technology. Cambridge: Woodhead. 276 p.
- [14] Prevorsek D, Oswald H (1990) Melt-spinning of PET and nylon fibers. In: Schultz J, Fakirov F, editors. Solid state behavior of linear polyesters and polyamides. Englewood Cliffs: Prentice Hall.
- [15] Chu B, Hsiao B (2001) Small-Angle X-ray Scattering of Polymers. *Chemical Reviews*. j. 101:1727-1761.
- [16] Mandelkern L (2002) Crystallization of Polymers – Volume 1 equilibrium concepts. Cambridge: University Press. 448 p.
- [17] Fließbach T (2006) Statistische Physik. München: Elsevier. 408 p.
- [18] Strobl G, Cho T (2007) Growth kinetics of polymer crystals in bulk. *European Physics Journal*. j. 23:55-65.
- [19] Banik N, Boyle F, Sluckin T, Taylor P (1979) Theory of structural phase transitions in poly(vinylidene fluoride). *Physical Review Letters*. j. 43: 456-460.
- [20] Strobl G (2007) A multiphase model describing polymer crystallization and melting. *Lecture Notes in Physics*. j. 714: 481-502.
- [21] Frick A, Stern C (2006) DSC-Prüfung in der Anwendung. München: Hanser. 164 p.
- [22] Schawe J, Hütter T, Heitz C, Alig I, Lellinger D (2006) Stochastic temperature modulation: A new technique in temperature-modulated DSC. *Thermochimica Acta*. j. 446:147-155.
- [23] Cheng S (2002) Handbook of Thermal Analysis and Calorimetry, Volume 3: Applications to Polymers and Plastics. Amsterdam: Elsevier. 828 p.

- [24] Hatakeyama T, Quinn F (2000) *Thermal Analysis: Fundamentals and Applications to Polymer Science*. London: Wiley.
- [25] LyondellBasell (2009) Product Data and Technical Information Moplen HP561R. Rotterdam: LyondellBasell.
- [26] BASF Corporation (2011) Datasheet Ultramid B24N03. Ludwigshafen: BASF Corporation.
- [27] Invista Resins & Fibers GmbH (2009) Product Specification Polyester Chips 4048. Gersthofen: Invista Resins & Fibers GmbH.
- [28] Hsiao B (2011) Polymorphism, Preferred Orientation and Morphology of Propylene-Based Random Copolymer Subjected to External Force Fields (dissertation). State University of New York at Stony Brook.
- [29] Liu Y, Cui L, Guan F, Gao Y, Hedin NE, Zhu L, Fong H (2007) Crystalline Morphology and Polymorphic Phase Transitions in Electrospun Nylon 6 Nanofibers. *Macromolecules*. j. 40:6283-6290.
- [30] Drobny J (2001) *Technology of fluoropolymers*. Boca Raton: CRC Press. 227 p.
- [31] Nalwa H (1995) *Ferroelectric Polymers – Chemistry, Physics and Applications*. New York: Marcel Dekker. 912 p.
- [32] Herbert J (1982) *Ferroelectric transducers and sensors*. New York: Gordon and Breach. 464 p.
- [33] Lovinger A (1983) Poly(vinylidene fluoride). *Developments in Crystalline Polymers*. j. 1:195.
- [34] Takahashi Y, Matsubara Y, Tadokoro H (1983) Crystal structure of form II of poly(vinylidene fluoride). *Macromolecules*. j. 16:1588-1792.
- [35] Hasegawa R, Takahashi Y, Chatani Y, Tadokoro H (1972) Crystal structures of three crystalline forms of poly(vinylidene fluoride). *Polymer Journal*. j. 3:600-610.
- [36] Weinhold S, Litt M, Lando J (1980) The crystal structure of the gamma phase of poly(vinylidene fluoride). *Macromolecules*. j. 13: 1178-1183.
- [37] Takahashi Y, Tadokoro H (1980) Crystal structure of form III of poly(vinylidene fluoride)
- [38] Wang T, Herberg J, Glass A (1988) *The Application of Ferroelectric polymers*. Glasgow: Blackie and Son. 304 p.
- [39] Du C, Zhu B, Xu Y (2007) Effect of stretching on crystalline phase structure and morphology of hard elastic PVDF fibers. *Journal of Applied Polymer Science*. j. 104:2254-2259.
- [40] Steinmann W, Walter S, Seide G, Gries T, Roth G, Schubnell M (2011) Structure, properties, and phase transitions of melt-spun poly(vinylidene fluoride) fibers. *Journal of Applied Polymer Science*. j. 120:21-35.
- [41] Lund A, Hagström B (2010) Melt-spinning of Poly(vinylidene fluoride) Fibers and Influence of Spinning Parameters on β -phase crystallinity. *Journal of Applied Polymer Science*. j. 116:2685-2693.

- [42] Walter S, Steinmann W, Schütte J, Seide G, Gries T, Roth G, Wierach P, Sinapius M (2011) Characterisation of piezoelectric PVDF monofilaments. *Materials Technology*. j. 26:140-145.
- [43] Solvay Solexis (2003) SOLEF 1006 PVDF Homopolymer (data sheet). Brussels: Solvay.
- [44] Hougham G (1999) *Fluoropolymers – Volume 2 Properties*. New York: Kluwer. 408 p.
- [45] Grady B (2011) *Carbon Nanotube Polymer Composites*. Hoboken: Wiley. 352 p.
- [46] Lee S, Kim M, Kim S, Youn J (2008) Rheological and electrical properties of polypropylene/MWCNT composites prepared with MWCNT masterbatch chips. *European Polymer Journal*. j. 44:1620-1630.
- [47] Wescott J, Kung P, Maiti A (2006) Conductivity of carbon nanotube polymer composites. *Applied Physics Letters*. j. 90.
- [48] Alig I, Pötschke P, Pegel S, Dudkin S, Lellinger D (2008) Plastic composites containing carbon nanotubes: Optimisation of processing conditions and properties. *Rubber Fibre Plastics*. j. 3:92-95.
- [49] Steinmann W, Walter S, Seide G, Gries T (2011) Melt spinning of electrically conductive bicomponent fibers. In: Adolphe D, Schacher L, editors: 11th World Textile Conference AUTEX 2011, 8-10 June 2011, Mulhouse, France. Book of Proceedings, Volume 2. Mulhouse : Ecole Nationale Supérieure d'Ingenieurs Sud-Alsace. pp. 716-721.
- [50] Wulfhorst J, Steinmann W, Walter S, Seide G, Heidelmann M, Weirich T, Gries T (2011) Nanoadditivation of meltspun filament yarns. In: ICONTEX 2011 International Congress of Innovative Textiles, 20-22 October 2011. Çorlu/Tekirdağ : Namik Kemal University. pp. 39-39.
- [51] Wulfhorst J, Steinmann W, Walter S, Seide G, Gries T (2011) Antibacterial behaviour and electrical conductivity of textiles by melt spinning of yarns with incorporated nanoparticles. In: Lahlou M, Koncar V, editors: Book of Abstracts / 3rd Edition of the International Conference on Intelligent Textiles and Mass Customisation ITMC'2011, October 27, 28 & 29, 2011, Casablanca & Marrakesh, Morocco. Casablanca: ESITH . p. 33.
- [52] Skrifvars M, Soroudi A (2009) Melt Spinning of Carbon Nanotube Modified Polypropylene for Electrically Conducting Nanocomposite Fibers. *Solid State Phenomena*. j. 151:43-47.
- [53] Liu K, Sun Y, Lin X, Zhou R, Wang J, Fan S, Jiang K (2010) Scratch-resistant, highly conductive and high-strength carbon nanotubes-based composite yarn. *ACS Nano*. j. 10:5827-5834.
- [54] Kyrylyuk A, Hermant M, Schilling T, Klumperman B, Koning C, van der Schoot P (2011) rolling electrical percolation in multicomponent carbon nanotube dispersions. *Nature Nanotechnology*. j. 6:364-369.

- [55] LyondellBasell (2011) Product Data and Technical Information Moplen HP561R.
Rotterdam: LyondellBasell.

IntechOpen

IntechOpen